Vol. 56: 261–280, 2013
doi: 10.3354/cr01157

CLIMATE RESEARCH
Clim Res

Published online May 16

Projection of multi-site daily temperatures over the Montréal area, Canada

D. I. Jeong[1,*], A. St-Hilaire[2], T. B. M. J. Ouarda[2,3], P. Gachon[1,4]

[1]Centre ESCER Université du Québec à Montréal, 201 Ave. President-Kennedy, Montréal, Québec H3A 2K6, Canada
[2]INRS-ETE, University of Québec, 490 de la Couronne Street, Québec G1K 9A9, Canada
[3]Water and Environmental Engineering, Masdar Institute of Science and Technology, PO Box 54224, Abu Dhabi, UAE
[4]Atmospheric Science and Technology Directorate, Canadian Centre for Climate Modeling and Analysis (CCCMA) section, Climate Research Division, Environment Canada, 800 de la Gauchetiere West, Office 7810, Montréal, Québec H5A 1L9, Canada

ABSTRACT: This study presents a post-adjustment procedure for a multivariate multi-site statistical downscaling model (MMSDM) which can simultaneously downscale multiple predictands at multiple observation sites by combining multivariate multiple linear regression and the stochastic randomization procedure. In the post-adjustment procedure, bias and determinant adjustment factors correct the systematic bias on the downscaled series using atmosphere-ocean coupled global climate model (AOGCM) predictors, and prevent the propagation of systematic error to the projected future predictands. The MMSDM with the post-adjustment procedure is applied to project a realistic series of 2 predictands (daily T_{max} and T_{min}) for 10 observation sites in the region of Montréal (southern Québec, Canada). The Canadian CGCM3 reference outputs (1961–2000) and future outputs under the A1B and A2 SRES scenarios (2061–2100) were employed as AOGCM predictors. On average over the 10 observation sites, the monthly means of the daily T_{max} and T_{min} were increased by 2.0–4.7 and 2.7–5.4°C while seasonal 90th percentile of daily T_{max} and 10th percentile of daily T_{min} (T_{max}90 and T_{min}10) were increased by 2.1–4.5 and 2.7–5.8°C for the A1B and A2 scenarios with the MMSDM, respectively. Future T_{max} and T_{min} series showed higher increases in winter than in the other seasons, as anticipated from AOGCMs or regional climate models over the same area. The average diurnal temperature ranges of future series suggest small increases in spring and autumn. Finally, the projected series yielded frost seasons that are 23 and 28 d shorter, whereas 23 and 27 more days are projected for the length of the growing season than in the present-day climate series.

KEY WORDS: Extreme event · Multi-site statistical downscaling · Projected temperatures · Southern Québec

1. INTRODUCTION

De-biased projections of climate changes on a targeted local or regional area are essential for research on impacts and potential adaptation to climate change, and for associated assessments in agriculture, forestry, water resource management, the natural environment, human health, and economy. Over the past few decades, many studies and reports have projected potential climate-change effects on temperatures over broad continental areas (e.g. Cubasch et al. 2001, Lobell et al. 2007, Meehl et al. 2007, Schoof et al. 2007) and over regional areas (e.g. Giorgi et al. 2001, Christensen et al. 2007, Gachon & Dibike 2007). To prepare realistic adaptation strategies for a target region, future climate-change scenarios should incorporate not only means and natural variability (Tett et al. 1997) but also spatial coherence between multiple surface observation sites.

*Email: jeong@sca.uqam.ca

Many studies (e.g. Katz & Brown 1992, Meehl et al. 2000, Cubasch et al. 2001) have focused on changes in future weather variability and extreme events since the early 1990s. Changes in variance and extreme events of temperature should significantly affect the overall aspects of a local society (Easterling 1999, Walther et al. 2002, IPCC 2012). Several studies (e.g. Bell et al. 2004, Tebaldi et al. 2006) have illustrated the changes in extreme temperatures due to future climate changes. These changes in extreme events may be detectable from reproduced and projected weather variability on present and future climate change scenarios, respectively.

AOGCMs (see Table 1 for abbreviations) provide future climate information on a coarse-scale global grid (generally >2° latitude × 2° longitude) for a number of variables (e.g. wind, temperature, humidity, and air pressure) forced by scenarios of varying concentrations of greenhouse gases and aerosols in the atmosphere. Dynamical (i.e. regional climate models, RCMs) or statistical downscaling techniques are then applied using the global-scale AOGCM outputs as boundary conditions to project future meteorological and climatological conditions in the targeted local or regional area at a higher resolution than the AOGCM. Statistical downscaling models (SDMs) are usually classified in 3 main groups: regression-based, stochastic weather generation, and weather typing models. The present study focuses on the regression-based statistical downscaling techniques.

Table 1. Abbreviations used in this paper. 'Statistics and indices': diagnostic indices from the daily maximum and minimum temperatures (T_{max} and T_{min}) values used to evaluate the performance of the statistical downscaling methods (source: Hessami et al. 2008). Square brackets: unit; time scale

Abbreviation	Expansion
General	
AOGCM	Atmosphere-ocean coupled global climate model
ASD	Automated regression-based statistical downscaling model developed by Hessami et al. (2008)
BAF	Bias adjustment factor
BCM2.0	Bergen Climate Model (BCM) Version 2
CCCSN	Canadian Climate Change Scenarios Network
CGCM3	Canadian coupled global climate model, version 3.1
CRCM	Canadian Regional Climate Model
CSIRO	Commonwealth Scientific and Industrial Research Organization
DAF	Determinant adjustment factor
DJF, MAM, JJA, SON	Winter, spring, summer, autumn (according to months)
INMCM	Institute for Numerical Mathematics
MIROC	Model for Interdisciplinary Research on Climate
MMLR	Multivariate multiple linear regression
MMSDM	Multivariate multi-site statistical downscaling model
NC	National Centers for Environmental Prediction/National Center for Atmospheric Research
NCARPCM	National Center for Atmospheric Research Parallel Climate Model
RCM	Regional climate model
SDM	Statistical downscaling model
SDSM	Regression-based SDM developed by Wilby & Dawson (2004)
T_{max}, T_{min}, T_{mean}	Maximum, minimum, mean temperature
SSDM	Single-variable single-site SDM
Model and predictor combinations	
C_A1B(M)	MMSDM with CGCM3 A1B predictors
C_A2(M)	MMSDM with CGCM3 A2 predictors
C_h(M)	MMSDM with CGCM3 historical predictors
NC(M)	MMSDM with NC predictors
NC(S)	SSDM with NC predictors
Statistics and indices	
Mean T_{max}	Mean of daily T_{max} [°C; mo]
SD T_{max}	Standard deviation of daily T_{max} [°C; mo]
Mean T_{min}	Mean of daily T_{min} [°C; mo]
SD T_{min}	Standard deviation of daily T_{min} [°C; mo]
$T_{max}90$	90th percentile of daily T_{max} [°C; season]
$T_{min}10$	10th percentile of daily T_{min} [°C; season]
HD90	Percentage of hot days with daily T_{max} >90th percentile T_{max} of 30 yr climate period (1971–2000) [%; summer, JJA]
CD10	Percentage of cold days with daily T_{min} <10th percentile T_{min} of 30 yr climate period (1971–2000) [%; winter, DJF]
DTR	Mean of diurnal temperature range [°C; season]
FSL	Frost season length: T_{min} <0°C more than 5 d [d; yr]
GSL	Growing season length: T_{mean} >5°C more than 5 d & T_{mean} <5°C more than 5 d [d; yr]

Usually, the empirical relationships between observed (or reanalyzed) atmospheric variables (predictors) and surface climate variables (predictands) in regression-based SDMs are driven by linear or nonlinear transfer functions. However, predictors from AOGCMs cannot fully incorporate all the features of atmospheric variables necessary for equivalence with the reanalysis predictors; thus, errors are generated between the downscaled time series from reanalysis predictors during the SDM calibration period, as well as those from AOGCM predictors. These errors also propagate to the projected scenarios from future AOGCM predictors. Therefore, post-adjustment procedures have been proposed in various studies to prevent the propagation of the errors to project future scenarios of predictands. As examples, Wilby & Dawson (2004) suggested a post-adjustment scheme based on bias correction and variance inflation factors for their regression-based SDM (named SDSM) used for a single observation site. Hessami et al. (2008) applied a very similar post-adjustment scheme for their single-site automated regression-based statistical downscaling (ASD) model. For single-site downscaling, they estimated 2 factors to adjust the deterministic component of a downscaled predictand from AOGCM predictors to obtain means and variances similar to those of the observed values, during the calibration of the downscaling model (with respect to the values of the reanalysis predictors). However, the post-adjustment procedure was not extended for multivariable (e.g. daily maximum and minimum temperatures, T_{max} and T_{min}) multi-site downscaling problems. Even though the proportion of explained variability from large-scale reanalysis predictors to unexplained variability reproduced by random noise can be determined based on a randomization assumption (see von Storch 1999), the proportion was not preserved for the downscaled outputs from AOGCM predictors in their adjusting procedure. In the present study, the primary objective was to improve the post-adjustment scheme of the regression-based SDM to project multisite daily T_{max} and T_{min}. Jeong et al. (2012d, 2013) illustrated the necessity for a post-adjustment procedure to project future daily precipitation occurrences and amounts at multiple sites. Their transfer function with atmospheric predictors explained much less variability of observed daily precipitation occurrences and amounts than those of temperatures (see Jeong et al. 2012c).

Based on stochastic weather generators, SDMs to generate multivariate climate variables (Kilsby et al. 2007) and their spatial coherence (Mehrotra & Sharma 2007, Burton et al. 2008) have already been suggested. Using a weather typing approach, Fowler et al. (2005) developed a multisite stochastic rainfall model. The present study employs a multivariate (i.e. daily T_{max} and T_{min}) multi-site statistical downscaling model (MMSDM) suggested by Jeong et al. (2012c) to project future temperature series. The MMSDM reproduces cross-site correlations among multisite surface predictands for a region and at-site correlations between multiple predictands at each observation site of the region based on the reanalysis predictors. The main goals of this study were to provide a randomization procedure with a modified post-adjustment scheme for the MMSDM, and to project future daily T_{max} and T_{min} using the MMSDM at multiple observation sites within a region from future AOGCM predictors. The MMSDM is applied to observation sites located in the greater Montréal area in Québec, Canada. In the targeted region, projections of multisite daily temperatures are essential to analyze regional or local climate change impacts on spring (snowmelt-generated) floods (Huziy et al. 2012), public health risks such as heat waves (Vescovi et al. 2005), and risks to the integrity of aquatic habitat (e.g. by modifying the thermal regime of rivers; Jeong et al. 2012a). RCM resolutions (generally larger than 30 km) are still considered too coarse for local site-scale impact studies (Wilby & Dawson 2004, Khalili et al. 2013). RCM simulations often have considerable biases, which have led to the development of a number of bias correction approaches to provide more realistic climate simulations for impact studies or local scale applications (see the recent studies over Europe by Maraun 2012 and Teutschbein & Seibert 2012; and over eastern North America by Roy et al. 2012). In our study, future simulated daily temperatures series were derived from the Canadian AOGCM version 3, i.e. the CGCM3 model, using predictors to project changes including extreme values. The results of the MMSDM using the post-adjustment scheme developed in this study were compared to those of a univariate single-site SDM with a previously developed post-adjustment scheme, i.e. the one adopted for the SDSM and ASD models.

2. METHODS

2.1. Statistical downscaling model

The MMSDM was first calibrated using observed meteorological data and reanalysis products as predictors. The National Centers for Environmental Prediction/National Center for Atmospheric Re-

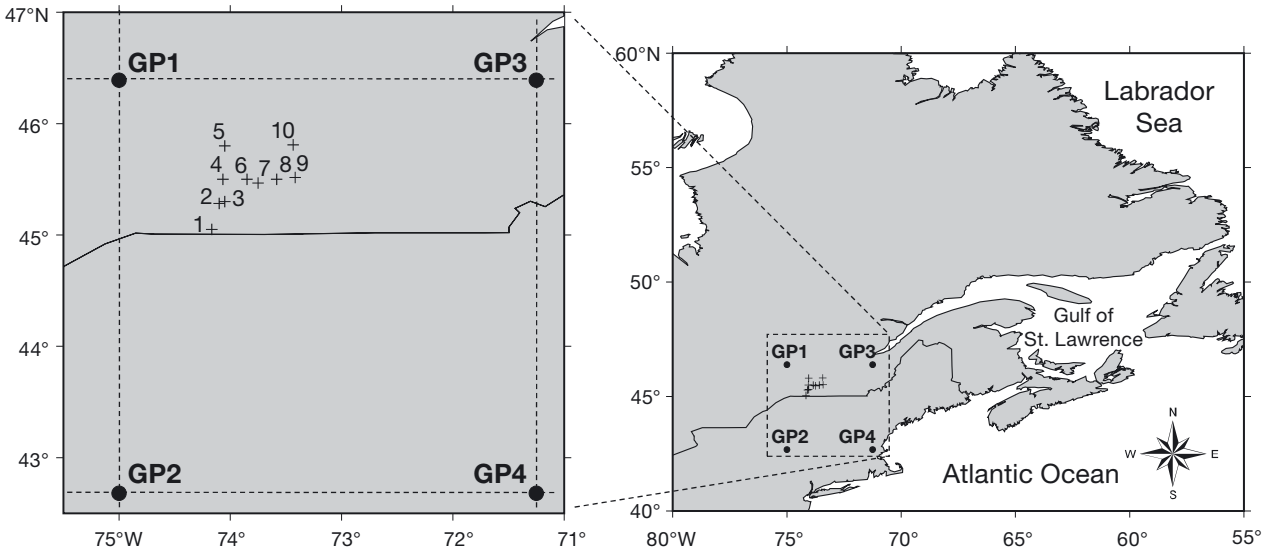

Fig. 1. Meteorological observation sites and CGCM3 grid points located near the sites. Numbers from 1 to 10 represent the meteorological observation sites (see Table 2), and GP1–GP4 represent CGCM3 grid point centroids

search (NCEP/NCAR; hereinafter NC; e.g. Kalnay et al. 1996) reanalysis data are one of the main sources of global-scale predictor variables. The reanalysis data are expected to be a representation of outputs from a 'perfect AOGCM' (Cannon & Whitfield 2002). The SDM calibrated with the NC reanalysis predictors was then applied in the second step to the CGCM3 current and future predictors to generate local climate change information of the same predictands (i.e. daily T_{max} and T_{min}) over the greater Montréal area in Québec, Canada (Fig. 1).

The MMSDM has 2 main procedures: a deterministic regression and a stochastic randomization (Jeong et al. 2012c). In the deterministic regression procedure, daily T_{max} and T_{min} (multiple predictand variables) at multiple observation sites in a region are simultaneously downscaled from NC predictors using the following multivariate multiple linear regression (MMLR) equation:

$$\hat{\mathbf{T}}^{NC} = \hat{\boldsymbol{\beta}}_0 + \mathbf{X}^{NC}\hat{\boldsymbol{\beta}} \quad (1)$$

where the matrix $\hat{\mathbf{T}}^{NC}[n \times 2m]$ contains the deterministic T_{max} and T_{min} values downscaled from NC predictors on a day (n = 1, 2, …, n) at a site (m = 1, 2, …, m). $\mathbf{X}^{NC}[n \times k]$ is the matrix of k normalized NC predictor variables. The matrix of constant terms $\hat{\boldsymbol{\beta}}_0[n \times 2m]$ and the parameter matrix $\hat{\boldsymbol{\beta}}[k \times 2m]$ are MMLR parameters estimated using the ordinary least square estimation method.

However, there are 3 main problems with the daily T_{max} and T_{min} at multiple observation sites downscaled by MMLR: (1) they can explain only a fraction of the observed variability in the daily T_{max} and T_{min}, (2) they cannot reproduce spatial dependence among cross-site T_{max} and among cross-site T_{min}, and (3) they cannot reproduce the at-site correlation between T_{max} and T_{min}. Therefore, unexplained variance, cross-site correlation, and at-site correlation in the daily T_{max} and T_{min} by MMLR are adjusted using the stochastic randomization procedure.

The residual matrix $\mathbf{E}^{NC}[n \times 2m]$ of the MMLR model for daily T_{max} and T_{min} is described below:

$$\mathbf{E}^{NC} = (\mathbf{T}^{O} - \hat{\mathbf{T}}^{NC}) \quad (2)$$

where $\mathbf{T}^{O}[n \times 2m]$ is the observed matrix, and $\hat{\mathbf{T}}^{NC}[n \times 2m]$ is the matrix of daily T_{max} and T_{min} by downscaled MMLR. To reproduce the variability in a daily T_{max} or T_{min} series and cross-site and at-site correlations among T_{max} and T_{min} series, the residual matrix $\tilde{\mathbf{E}}^{NC}[n \times 2m]$ is generated from a multivariate normal distribution having an error mean equal to 0 and an error covariance matrix [$\Sigma^{NC} = \mathbf{S}^{NC}\mathbf{R}^{NC}\mathbf{S}^{NC}$] equal to that of the residual matrix $\mathbf{E}^{NC}[\tilde{\mathbf{E}}^{NC} \sim \mathbf{N}_{2m}(0, \Sigma^{NC})]$, under the assumption that the residual follows a Gaussian distribution. Here, $\mathbf{S}^{NC}$ is a diagonal matrix of standard deviations, and $\mathbf{R}^{NC}$ is a correlation matrix of the residual matrix $\mathbf{E}^{NC}$. The residuals thus generated are then added to the downscaled deterministic temperature matrix $\hat{\mathbf{T}}^{NC}$ to form a new matrix:

$$\tilde{\mathbf{T}}^{NC} = \hat{\mathbf{T}}^{NC} + \tilde{\mathbf{E}}^{NC} \quad (3)$$

where $\tilde{\mathbf{E}}^{NC}[n \times 2m]$ is the residual matrix generated from the multivariate normal distribution, and $\tilde{\mathbf{T}}^{NC}[n$

× 2m] is the matrix of daily T_{max} and T_{min} series generated by the MMSDM approach and NC predictors.

2.2. Projection of future scenarios

From Eq. (2), the variance and standard deviation of the residual of a predictand downscaled from NC predictors can be described as follows:

$$\mathbf{e}^{NC} = \mathbf{t}^{O} - \hat{\mathbf{t}}^{NC} \quad (4a)$$

$$\mathrm{var}(\mathbf{e}^{NC}) = \mathrm{var}(\mathbf{t}^{O}) - \mathrm{var}(\hat{\mathbf{t}}^{NC}) - 2\mathrm{cov}(\hat{\mathbf{t}}^{NC}, \mathbf{e}^{NC}) \quad (4b)$$

$$S^{NC} = \sqrt{V^{O} - V^{NC}} \quad (4c)$$

where $\mathbf{e}^{NC}$, $\mathbf{t}^{O}$, and $\hat{\mathbf{t}}^{NC}$ are [n × 1] vectors of the residual, observation, and downscaled deterministic series of an observation site. V^{O}(= var($\mathbf{t}^{O}$)) and V^{NC}(= var($\hat{\mathbf{t}}^{NC}$)) are the variances of the vectors $\mathbf{t}^{O}$ and $\hat{\mathbf{t}}^{NC}$, and cov($\hat{\mathbf{t}}^{NC}$, $\mathbf{e}^{NC}$) is equal to 0. S^{NC} is the standard deviation of the residual vector $\mathbf{e}^{NC}$. Using S^{NC}, a residual element $\tilde{e}_i^{NC}$ of the vector $\tilde{\boldsymbol{e}}^{NC}$ is generated:

$$\tilde{e}_i^{NC} = z_i S^{NC} + b^{NC} \quad (5a)$$

$$b^{NC} = M^{O} - M^{NC} = 0 \quad (5b)$$

where z_i is the random variable generated from the standard normal distribution, M^{O} and M^{NC} are the means of the vectors $\mathbf{t}^{O}$ and $\hat{\mathbf{t}}^{NC}$, and b^{NC} is a bias between vectors $\mathbf{t}^{O}$ and $\hat{\mathbf{t}}^{NC}$. Usually, the bias b^{NC} is equal to 0 because the parameter matrix $\hat{\boldsymbol{\beta}}$ of the MMLR is a best linear unbiased estimator. As explained previously, the residual matrix $\tilde{\mathbf{E}}^{NC}[n \times 2m]$ is generated from the multivariate normal distribution $\tilde{\mathbf{E}}^{NC} \sim \mathbf{N}_{2m}(0, \Sigma^{NC})$.

The calibrated MMSDM is then applied to the AOGCM historical predictors $\mathbf{X}^{H}[n \times k]$, which are simulated outputs from an AOGCM model under the historical greenhouse gas and aerosol concentrations. The downscaled deterministic part of predictand matrix $\mathbf{T}^{H}[n \times 2m]$ from the predictors $\mathbf{X}^{H}$ requires an adjustment because of the difference between $\mathbf{X}^{NC}$ and $\mathbf{X}^{H}$. A predictand vector $\mathbf{t}^{H}$ in the matrix $\mathbf{T}^{H}$ is adjusted as shown:

$$\hat{\mathbf{t}}^{H} = \mathbf{t}^{H}\sqrt{\frac{V^{NC}}{V^{H}}} \quad (6)$$

where V^{H} is the variance of the vector $\mathbf{t}^{H}$ of an observation site. The determinant adjustment factor (DAF) $\sqrt{V^{NC}/V^{H}}$ inflates or deflates the deterministic series of the downscaled vector $\mathbf{t}^{H}$; therefore, the adjusted vector $\hat{\mathbf{t}}^{H}$ has the same variance as the vector $\hat{\mathbf{t}}^{NC}$.

A residual element $\tilde{e}_i^{H}$ of the vector $\tilde{\mathbf{e}}^{H}$ for each predictand is generated as below:

$$\tilde{e}_i^{H} = z_i S^{NC} + b^{H} \quad (7a)$$

$$b^{H} = M^{NC} - M^{H} \quad (7b)$$

where M^{H} is the mean value of the vector $\hat{\mathbf{t}}^{H}$, and b^{H} is a bias between the vectors $\hat{\mathbf{t}}^{NC}$ and $\hat{\mathbf{t}}^{H}$. Herein, the term b^{H} is called the bias adjustment factor (BAF); it is obviously a non-zero value due to the difference between $\mathbf{X}^{NC}$ and $\mathbf{X}^{H}$. The DAF and BAF are employed to prevent the propagation of systematic error originating from the difference between the NC and AOGCM predictors in the future scenarios for the predictands. The residual matrix $\tilde{\mathbf{E}}^{H}[n \times 2m]$ is generated from the multivariate normal distribution $\tilde{\mathbf{E}}^{H} \sim \mathbf{N}_{2m}(\mathbf{b}^{H}, \Sigma^{NC})$ to reproduce at-site or cross-site correlations between the T_{max} and T_{min} at multiple observation sites within a region; here, the matrix $\mathbf{b}^{H}[1 \times 2m]$ is the BAF vector. The matrix $\tilde{\mathbf{E}}^{H}$ is added to the adjusted deterministic matrix $\hat{\mathbf{T}}^{H}[n \times 2m]$ to generate the AOGCM historical scenario matrix $\tilde{\mathbf{T}}^{H}[n \times 2m]$, as described by Eq. (3).

Future deterministic component series of the predictand matrix $\mathbf{T}^{F}[n \times 2m]$ is produced by the parameter matrix of the MMLR in Eq. (1) and the AOGCM future predictor matrix $\mathbf{X}^{F}[n \times k]$, which are the simulated outputs from an AOGCM model under future emission scenarios during a target period. Again, the generated matrix $\mathbf{T}^{F}$ requires an adjustment procedure by the DAF, as follows:

$$\hat{\mathbf{t}}^{F} = \mathbf{t}^{F} \times DAF \quad (8)$$

where $\mathbf{t}^{F}[n \times 1]$ is a predictand vector in the matrix $\mathbf{T}^{F}$ and the DAF is $\sqrt{V^{NC}/V^{H}}$. Again, the random noise matrix $\tilde{\mathbf{E}}^{H}$ is added to the adjusted deterministic matrix $\hat{\mathbf{T}}^{F}[n \times 2m]$ to generate the AOGCM future scenario matrix $\tilde{\mathbf{T}}^{F}[n \times 2m]$, as described by Eq. (3).

The use of the DAF in this study constitutes its major difference from the adjustment procedures in the SDSM and ASD models. The 2 single-variable single-site statistical downscaling models (hereinafter, SSDMs) directly inflate the variance of the deterministic component $\mathbf{t}^{H}$, a vector of downscaled deterministic series of a predictand from the AOGCM predictors $\mathbf{X}^{H}$, using only random noise. A residual element e_i^{H} of the vector $\mathbf{e}^{H}$ for the SDSM and ASD models is expressed as:

$$e_i^{H} = z_i\sqrt{V^{O} - V^{H}} + b^{H} \quad (9)$$

The observed mean and variance of a predictand on a single site is reproduced by adding the residual vector $\mathbf{e}^{H}$ to the deterministic component $\mathbf{t}^{H}$ when the

variance of the deterministic series of the historical AOGCM predictors V^H is smaller than the variance in observations (V^O). The variance inflation methodology, however, cannot be applied when V^H is larger than V^O. Furthermore, this procedure ignores any difference between the variances of the deterministic component series with the NC predictors (V^{NC}) and that with the AOGCM predictors (V^H) during the historical calibration period. The uncontrolled variance should significantly affect the means and variances of future scenarios. The reproduction of cross-correlations among multi-site observations is also difficult when based on the uncontrolled deterministic component series derived from the AOGCM predictors.

2.3. Data and application

2.3.1. Study area and predictands

Fig. 1 shows the study area around the city of Montréal in southern Québec (Canada). Meteorological observation sites over Montréal and CGCM3 grid points located near the observation sites are also provided in Fig. 1. As surface predictands, this study employed daily T_{max} and T_{min} series from the 10 observation sites in the Montréal region. Table 2 reports the names and locations of the meteorological stations, mapped over southern Québec in Fig. 1. Ranges of annual means of daily T_{max} and T_{min} of the 10 observation sites are 10.2 to 12.1°C and 0.0 to 3.8°C during the 30 yr climate period (1971–2000), respectively. The site at the highest altitude, St-Jérôme, yields the lowest annual means of daily T_{max} and T_{min}. The selected Montréal area is the most populous region of Québec, and therefore, adaptation to climate change impact is of the utmost importance. However, the regional study area is relatively small. The distance between Site 1 and Site 10, the longest distance between any 2 of the 10 observation sites, is 102 km.

Table 2. Observation sites for the maximum and minimum temperatures from Environment Canada over the Montréal area

No.	Name of station	Latitude (°N)	Longitude (°W)	Altitude (m)
1	Huntingdon	45.05	74.17	49.1
2	Valleyfield	45.28	74.10	45.7
3	Les Cèdres	45.30	74.05	47.2
4	Oka	45.50	74.07	91.4
5	St-Jérôme	45.80	74.05	169.5
6	Ste-Geneviève	45.50	73.85	22.9
7	Montréal/PET Airport	45.47	73.75	35.7
8	Montréal/McGill	45.50	73.58	56.9
9	Montréal/St-Hubert Airport	45.52	73.42	27.4
10	L'Assomption	45.81	73.43	21.0

2.3.2. AOGCM predictors

We used AOGCM predictors from current and future climate scenarios simulated using the CGCM3.1 model to project current and future daily T_{max} and T_{min}. The CGCM3 model is an improvement on previous CGCM models, and the CGCM3.1 is a subsequent version of the initial CGCM3 (see Flato & Boer 2001). This version is the one used to produce an extensive suite of model simulations for use in the Intergovernmental Panel on Climate Change (IPCC) Fourth Assessment Report (IPCC 2007). The CGCM3.1 model is run at T47 and T62 resolutions, equivalent to surface grid resolutions of approximately 3.75° × 3.75° and 2.8° × 2.8°, respectively. They both provide outputs at 32 vertical levels, extended to 1 hPa (e.g. ~50 km above the surface). This study employed the CGCM3 T47 spectral truncation (hereafter CGCM3; see further information about this AOGCM version on the following Environment Canada website: www.ec.gc.ca/ccmac-cccma). CGCM3 historical predictors (using the historical greenhouse gas and aerosol concentrations), covering the period 1961–2000, and CGCM3 A1B and A2 predictors, covering the future period 2061–2100 following the SRES A1B and A2 scenarios (Nakicenovic et al. 2000), were used to project daily T_{max} and T_{min} series over the Montréal area.

Historical NC predictors were obtained from the NC reanalysis data (e.g. Kalnay et al. 1996, Kistler et al. 2001) for the period from 1961–2000. The NC reanalysis uses a T62 global spectral model to consistently collect observational data from a wide variety of observed sources. Details of the reanalysis project can be found in Kalnay et al. (1996). All details on the preparation of the potential predictors from NC reanalysis and the preprocessed data developed and obtained from the Canadian Climate Change Scenarios Network (CCCSN) project of Environment Canada (www.cccsn.ec.gc.ca) and corresponding documentation are available at: http://loki.qc.ec.gc.ca/DAI/predictors-e.html (see DAI CGCM3 Predictors, 2008). The NC predictors available for the downscaling experiment are enumerated in Table 3. The potential predictors are atmospheric circulation variables (e.g. the speed and U- and V-components of

Table 3. Selected predictors per month for both daily maximum and minimum temperatures (T_{max} and T_{min}) in a backward stepwise regression, where the selection frequency (i.e. the number of times selected) of the predictors at 4 different grid points is provided

Variables	Jan	Feb	Mar	Apr	May	Jun	Jul	Aug	Sep	Oct	Nov	Dec	Sum
Mean sea level pressure	2	1	2	2	2	1	2	2	1	2	1	2	20
1000 hPa													
Wind speed		2		1	2						1		6
U-component	1		1		1		2	1		2	1	2	11
V-component	1	1	1						1			1	5
Vorticity													
Divergence	3	2	2	1			1	1	1		2		13
Specific humidity	1	2	1	1	1	2	1	1	1	1	1	1	14
500 hPa													
Wind speed				1		2							3
U-component				1				1	2				4
V-component						1	1				1	2	5
Vorticity													
Geopotential	1			2	2			1		1	3	1	11
Divergence												1	1
Specific humidity						1	1		2			2	6
850 hPa													
Wind speed	1	2				1				1			5
U-component		1		1	1	2	2				1	1	9
V-component		2	1		1	1			1	1		1	8
Vorticity													
Geopotential	2	1	2	2	1	1	1	2	2	2	1	2	19
Divergence			1	1		1			1		1		5
Specific humidity	3	1	1	2	1	1		1	2	1	1	2	16
Sum	15	15	12	15	12	14	11	10	14	11	14	18	

wind, divergence, and vorticity at 500, 850, and 1000 hPa levels), mean sea level pressure, geopotential height (at 500 and 850 hPa levels), and specific humidity (at 500, 850, and 1000 hPa levels).

The selection of appropriate atmospheric predictor variables requires comprehensive consideration, because downscaling results are highly sensitive to the selection of predictor variables. The optimal predictors selected among the 84 NC variables (4 grid points with 21 predictors each) for the daily T_{max} and T_{min} of the 10 observation series were identified using a backward stepwise regression approach for each month, using the *F*-test as the criterion for predictor inclusion in the model at a confidence interval $\alpha = 0.01$ (a detailed description can be found in Jeong et al. 2012c). Backward stepwise regression was initiated with all predictors being part of the model, and statistically insignificant predictors were eliminated one after the other to avoid overfitting. Although there may be some colinearity remaining, the stepwise procedure typically avoids the joint selection of highly correlated predictors. Because of relatively long record lengths (50 to 90 times larger than the numbers of MMLR parameters), the calibrated MMLRs yielded similar performance on the calibration and validation data sets and did not show any overfitting problem (see the calibrated and validated performances of the MMLR presented in Figs. 3 & 4 of Jeong et al. 2012c). Table 3 reports the predictors selected for each month for the monthly MMLR equations from the initial 84 potential predictor variables at all 4 grid points. For each month, 10 to 18 atmospheric variables were selected as predictors for both daily T_{max} and T_{min}. Mean sea level pressure, geopotential height at 500 and 850 hPa, and specific humidity at 850 and 1000 hPa are the most fre-

quently selected predictors among the 21 reanalysis variables. Usually, variables at lower levels (i.e. 1000 and 850 hPa) are selected as predictors more frequently than those at the upper level (500 hPa). The selected predictors presented in Table 3 are relevant for downscaling daily T_{max} and T_{min} variables because they include several atmospheric circulation predictors and thermodynamic fields (e.g. wind speeds, U- and V-components, specific humidity, mean sea level pressure, and geopotential heights at different levels) physically related to daily temperatures (see further discussion by Gachon & Dibike 2007). The MMLR parameters for the daily T_{max} and T_{min} series are calibrated separately for each month using predictands and predictors from 1961–1990. To ensure stability and robustness in the stochastic randomization procedure of the statistical downscaling model, the MMSDM generated 50 realizations of temperature series of lengths equal to the historical period, from 1961–2000, and the future target period, from 2061–2100.

2.3.3. Statistics and extreme temperature indices

This study generally employed the same statistics and extreme temperature indices as in Hessami et al. (2008) to analyze climate change impacts on daily temperature series in the future. The means and standard deviations (SDs) of the downscaled daily T_{max} and T_{min} were calculated every month to compare the observed and downscaled values. Additionally, 7 temperature indices were employed to analyze the impacts of extreme daily temperature events in future climate-change scenarios. Temperature statistics and other indicies (see Table 1) were taken from Hessami et al. (2008). Temperature extremes are quantified by the 90th percentile of daily T_{max} and the 10th percentile of daily T_{min} ($T_{max}90$ and $T_{min}10$) in every season, i.e. spring (Mar, Apr, May: MAM), summer (Jun, Jul, Aug: JJA), autumn (Sep, Oct, Nov: SON), and winter (Dec, Jan, Feb: DJF). Temperature extreme spells are quantified by the percentages of hot and cold days (HD90 and CD10, respectively). The HD90 (CD10) is defined as the percentage of hot (cold) days with daily T_{max} (T_{min}) larger (smaller) than the 90^{th} (10^{th}) percentile T_{max} (T_{min}) of the 30 yr climate period from 1971–2000 in summer (winter). Frost season length (FSL) starts and ends when T_{min} is lower and higher than 0°C for 5 consecutive days, respectively. For the growing season length (GSL) index, daily mean temperatures (T_{mean}) are used, calculated as the average of T_{max} and T_{min}. GSL begins when T_{mean} exceeds 5°C for 5 consecutive days and ends after 5 consecutive days of temperatures below 5°C. These indices are also used here, as they are useful to evaluate the MMSDM tool not only on the mean values of downscaled temperatures but also on the seasonal variability and extreme features of daily T_{max} and T_{min} around key thresholds and durations (i.e. they are useful because of their application in a number of areas of impact research).

3. RESULTS

The future temperature series projected by the SDMs and CGCM3 future predictors are presented and discussed in this section. The SDMs generated 50 realizations of temperature series of lengths equal to the historical period, 1961–2000, and the target future period, 2061–2100. Hence, the results of the SDMs presented in this section are evaluated from the 50 realizations of daily T_{max} and T_{min} series. Note that the daily MMLR and the SDMs are calibrated separately for each month from 1961–1990, using the selected predictors presented in Table 3. The detailed descriptions of the calibration and validation of the MMSDM using the historical NC predictors are provided in Jeong et al. (2012c). The main objective of this study was to improve the effectiveness of the post-adjustment scheme of the regression-based SDM in projecting future daily T_{max} and T_{min} at multiple regional stations. Therefore, this section is focused on presenting the effects of the suggested post-adjustment scheme on the projected future temperature series and their extreme indices, with respect to the baseline period.

3.1. Adjustment factors

Fig. 2 reports the percentages of the variances in downscaled deterministic series explained by the MMLR model with NC predictors (V^{NC}s) for all 10 observation sites for each of the 12 months during the model calibration period from 1961–1990. The percentages of explained variance in daily T_{max} varied from 60 to 77%, whereas those for daily T_{min} varied from 58 to 77% for each month and each site. The percentages of explained variance of the T_{min} series by the MMLR are generally smaller and yield larger variability between stations than those of the T_{max} series. Linear transfer functions with reanalysis predictor usually explain less variance of daily T_{min} than daily T_{max} in the study area (see Hessami et al. 2008,

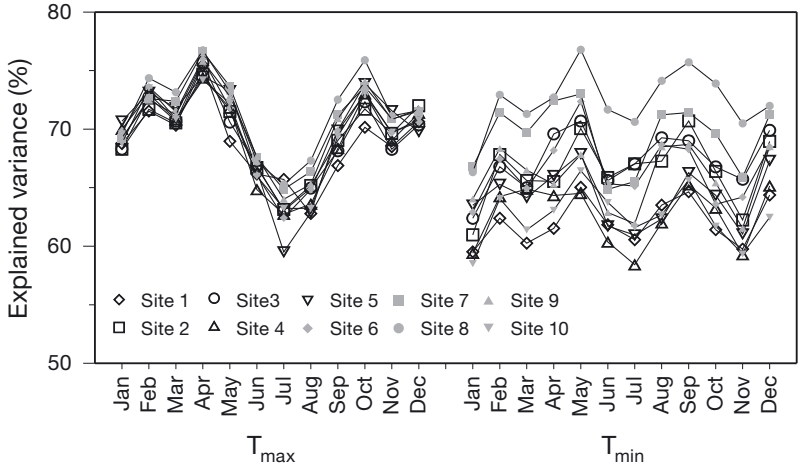

Fig. 2. Percentages of explained variances in the deterministic series of the predictands downscaled by the MMLR model with NC predictors (V^{NC}s) in the total variances of the observations (V^{O}s) for the 10 observation sites for all 12 months. Abbreviations in Table 1

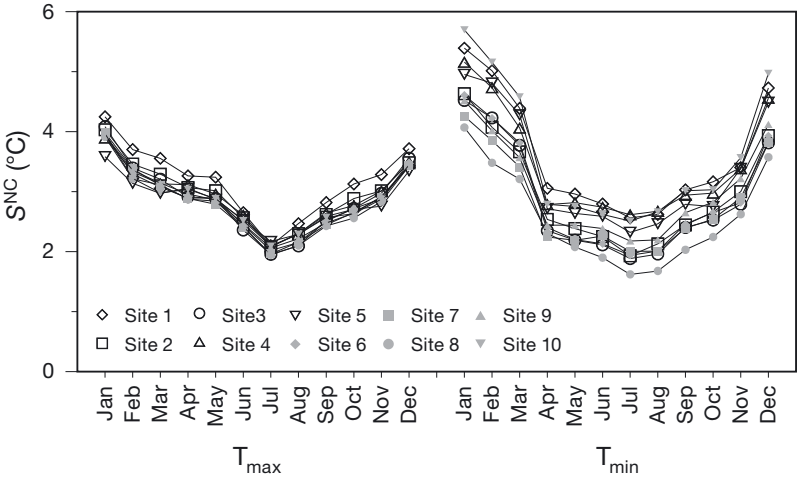

Fig. 3. Standard deviations of the residual series of the deterministic series downscaled by MMLR and the NC predictors (S^{NC}s) for the 10 observation sites for all 12 months. Abbreviations in Table 1

Jeong et al. 2012c). Daily T_{min} series have spatially weaker correlation than daily T_{max} series (see Fig. 5). The explained percentages of daily T_{max} show strong seasonal variability in each month but relatively small spatial variability among the 10 observation sites. The explained percentages of T_{max} are smaller in summer than in the other seasons. In contrast, the percentages of explained variance in daily T_{min} showed relatively smaller seasonal variability and larger spatial variability than those in daily T_{max}. Usually, daily T_{max} and T_{min} are more explainable by the NC predictors (i.e. specific humidity and geopotential height, and the U- and V-components at different levels) in winter than in summer in this region (Jeong et al. 2012b), as large-scale forcing factors (i.e. atmospheric circulation) play a larger role in winter than in summer. On average, Site 8 (McGill) showed the best performance, and Site 1 (Huntington) showed the worst performance with respect to both daily T_{max} and T_{min}.

Fig. 3 presents the SDs of the residuals of the series of predictands obtained from the deterministic series downscaled by MMLR with the NC predictors (S^{NC}, as given by Eq. 4c) for each observation site for all 12 months during the model calibration period. Again, the S^{NC} values showed strong seasonal variability in both T_{max} and T_{min} that was smaller in summer than in the other seasons. Even though the MMLR with the NC predictors explained less of the variance in the observations, the S^{NC} values are smaller in summer than those in the other seasons because the natural variability of daily T_{max} and T_{min} in summer is smaller. The strong seasonality of the S^{NC} values implies that the MMLR and randomization procedures should be calibrated with a consideration of seasonality. Again, the S^{NC} of the daily T_{min} values showed larger spatial variability than the daily T_{max} values.

Fig. 4 shows the BAFs and DAFs calculated from the deterministic component series downscaled by MMLR with the NC predictors and by MMLR with the CGCM3 historical predictors for each observation site for all 12 months during the model calibration period. The BAFs employed to adjust the means of the deterministic series generated by MMLR with the CGCM3 historical predictors are the same as those with the NC predictors. Note that the means of the deterministic series generated by MMLR with the NC predictors are the same as the observations because MMLR is a best linear unbiased estimator. The DAFs employed to adjust the variance of the deterministic series generated by MMLR with the CGCM3 historical predictors are also the same as those with the NC predictors. Note that systematic errors exist in the predictands generated by MMLR with the CGCM3 historical predictors because the MMLR

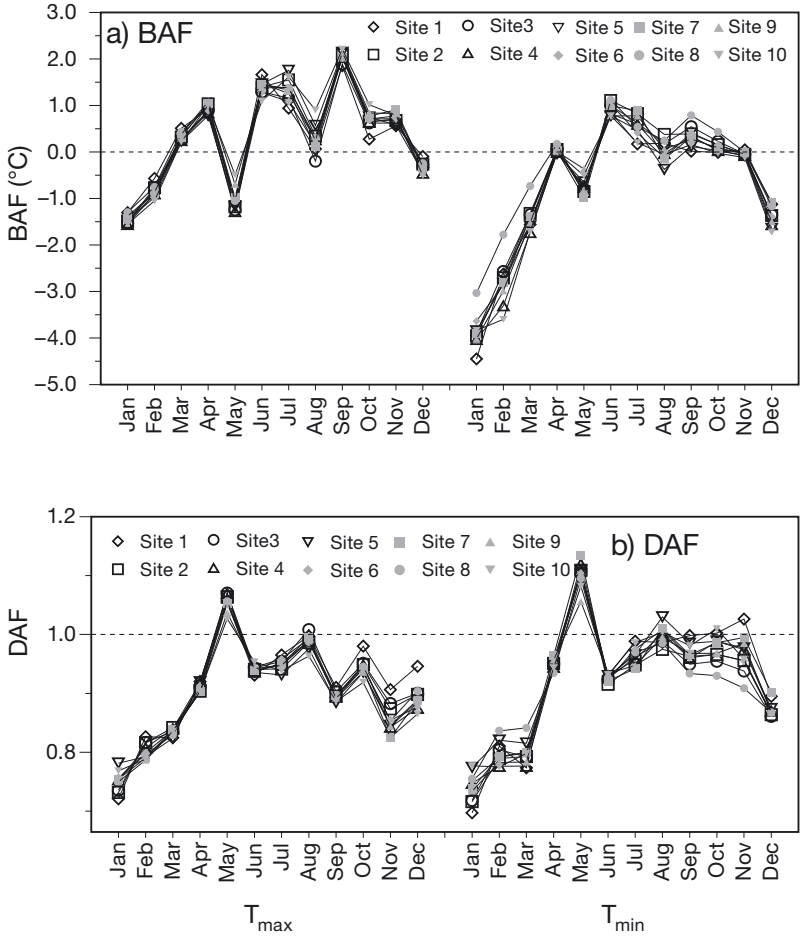

Fig. 4. (a) Bias adjustment factors (BAFs) and (b) determinant adjustment factors (DAFs) derived from deterministic component series of the predictands predicted by MMLR with the NC predictors and by MMLR with the CGCM3 historical predictors for the 10 observation sites for all 12 months. Abbreviations in Table 1

model is calibrated with the NC predictors, and the CGCM3 predictors cannot reproduce the NC predictors perfectly. As shown in Fig. 4a, the absolute values of the BAFs for T_{max} are larger in January, May, June, July, and September than in the other months, whereas those for T_{min} are larger in winter or colder months (i.e. from December to March) than in warmer months. As shown in Fig. 4b, most DAFs are <1. In particular, the factors yielded smaller values in January, February, and March than in the other months for both T_{max} and T_{min}. This result implies that the variances of the deterministic component series derived by MMLR with the CGCM3 historical predictors (V^{H}s) are larger than those with the NC predictors (V^{NC}s). Consequently, without a DAF correction factor, SDSM and ASD use a larger proportion of signal from large-scale AOGCM predictors but a lesser proportion of regional variability (i.e. from the residual element, see Eq. 9 and discussion in the Section 2) to project future daily T_{max} and T_{min} than those determined by the linear transfer function with NC predictors (especially in winter months). Therefore, the application of DAFs is mainly useful to project future temperature series to reduce the overestimation suggested in the variances of the deterministic component series derived by MMLR with the CGCM3 historical predictors (with respect to NC predictors). Furthermore, the V^{H}s values in January, February, and March are larger than the variances in the observations, V^{O}s (not shown). In the adjustment procedure used for the SDSM and ASD, the variance inflation methodology (i.e. the randomization procedure) is inapplicable in those cases (see Eq. 9).

3.2. Spatial and temporal coherence between T_{max} and T_{min}

Figs. 5 & 6 present the cross-site correlations of T_{max} and T_{min} and at-site correlation between T_{max} and T_{min}, respectively. In these figures, the observed series are compared with the series downscaled by the NC(S), NC(M), C_h(M), C_A1B(M), and C_A2(M) models explained in Table 1. Fig. 5 shows cross-site correlations between pairs of daily temperatures (T_{max} or T_{min}) as a function of interstation distance for all possible combinations of station pairs. The NC(M) and C_h(M) reproduced the observed cross-site correlation coefficient values for both T_{max} and T_{min} almost exactly using the multi-site randomization procedure developed in this study. The result also implies that the deterministic series from the CGCM3 historical predictors reproduced the cross-site correlations of the deterministic series from the NC predictors fairly well in terms of the selected predictor sets, as the NC(M) and C_h(M) employ the same randomization component. However, MMLR without a randomization procedure tended to overestimate the correlations, whereas NC(S) with a single-site (and uncorrelated) randomization procedure tended to underestimate these values in all cases. The cross-site correlations of

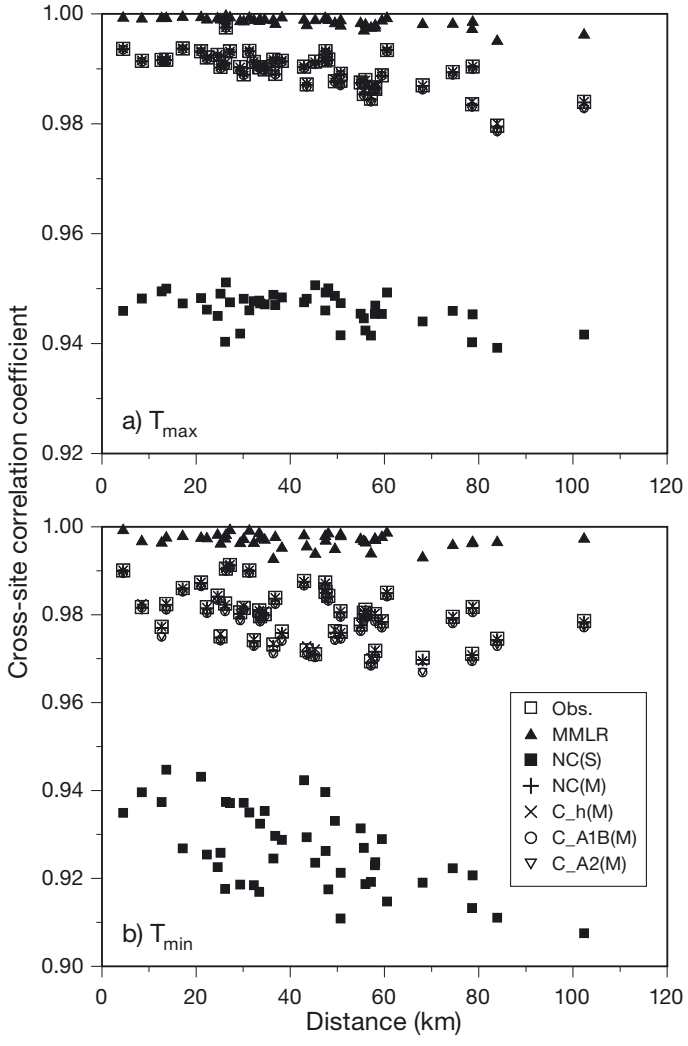

Fig. 5. Cross-site correlation coefficients of (a) T_{max} and (b) T_{min} between pairs of observations, MMLR, NC(S), NC(M), C_h(M), C_A1B(M), and C_A2(M) series versus their station distances for all possible combinations of station pairs, where MMLR, NC(S), NC(M), C_h(M), C_A1B(M), and C_A2(M) represent the series downscaled by MMLR with the NC predictors, by the SSDM with the NC predictors, by the MMSDM with the NC predictors, and by the MMSDM with the CGCM3 historical predictors and the series projected by the A1B and A2 predictors, respectively. Abbreviations in Table 1

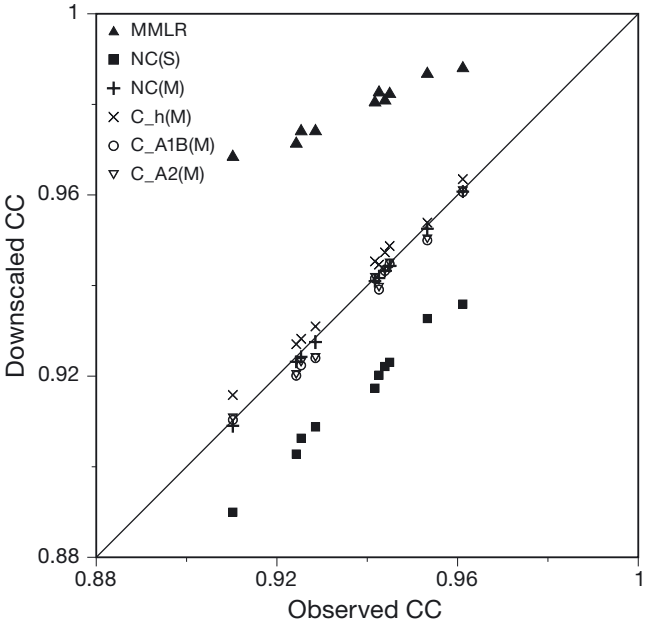

Fig. 6. At-site correlation coefficients (CCs) between daily T_{max} and T_{min} from the observations and the predicted MMLR, NC(S), NC(M), C_h(M), C_A1B(M), and C_A2(M) series for all stations, where MMLR, NC(S), NC(M), C_h(M), C_A1B(M), and C_A2(M) represent the series downscaled by MMLR with the NC predictors, by the SSDM with the NC predictors, by the MMSDM with the NC predictors, and by the MMSDM with the CGCM3 historical predictors and the series projected by the A1B and A2 predictors, respectively. Abbreviations in Table 1

C_A1B(M) and C_A2(M) are similar to those of the observations. Seasonally, both T_{max} and T_{min} yield weaker cross-site correlation coefficients in summer than in the other seasons (results not shown).

Fig. 6 presents the at-site correlation coefficients between daily T_{max} and T_{min} from the observations and the predicted MMLR, NC(S), NC(M), C_h(M), C_A1B(M), and C_A2(M) series for all stations. NC(M) and C_h(M) reproduced the at-site correlation coefficients of the observations almost exactly. However, MMLR overestimated them, and NC(S) underestimated these values for all sites. The at-site correlation values of the projected temperature scenarios by C_A1B(M) and C_A2(M) are almost the same as those of the observations.

3.3. Projected results of temperature statistics and indices

The effects of climate change on temperature statistics and indices (described in Table 1) are presented herein. The statistics and indices are calculated from the observed daily T_{max} and T_{min} series and downscaled series using the NC predictors and CGCM3 historical predictors (C_h) for the historical period from 1961–2000. They are also calculated from the projected daily T_{max} and T_{min} series given by the CGCM3 A1B and A2 predictors (C_A1B and C_A2) for the target period from 2061–2100. The MMSDM with the post-adjustment scheme suggested in this study and the SSDM with the previously employed post-adjustment scheme adopted by

the SDSM and ASD are applied to generate the C_h, C_A1B, and C_A2 scenarios. The statistics and extreme indices calculated from the C_h, C_A1B, and C_A2 scenarios of the 2 SDMs are then compared.

The monthly means and SDs of daily T_{max}, the 90th percentile of daily T_{max}, and the 10th percentile of daily T_{min} are presented in Figs. 7–10 for a representative site (7, Montréal) located in the middle of the study area. In these figures, the results with the NC and the MMSDM are not distinguishable from those of the SSDM because they are identical for these statistics at-site, although the cross-site correlations among multiple sites in the series downscaled by the 2 SDMs differ (see Fig. 5).

Fig. 7 presents the monthly means of the daily T_{max} of the observations and the NC and C_h, C_A1B, and C_A2 series derived with the MMSDM using the post-adjustment scheme developed in this study (denoted 'M' in the figures) and the SSDM with the post-adjustment scheme earlier employed by the SDSM and ASD (denoted 'S') for each month. For brevity, only results for January, March, May, July, September, and November are shown. The NC reproduced the observation variables very well for all months. Differences in the medians between the observations and the NC are smaller than 0.3°C for each month. The accurate reproduction with the NC implies that the stochastic downscaling model is well calibrated. Regarding the results by the MMSDM, C_h(M) reproduces the statistic well for each month. The result illustrates that the BAFs and DAFs presented in Fig. 4 adjust the biases and variances between predictands from the NC and CGCM3 historical predictors relatively well. The medians of the monthly means of daily T_{max} increased by 2.2 to 3.8°C with C_A1B(M) and by 3.0 to 4.6°C with C_A2(M) over those of C_h(M) for overall months. In winter and in April and May, the increases in the medians of the variables are larger than those in the other months. As for the results of the SSDM with the post-adjustment scheme previously adopted by the SDSM and ASD, C_h(S) also showed a similar reproduction ability to those of the C_h(M) in terms of medians. However, the increases in the monthly mean T_{max} of the future C_A1B(S) and C_A2(S) are

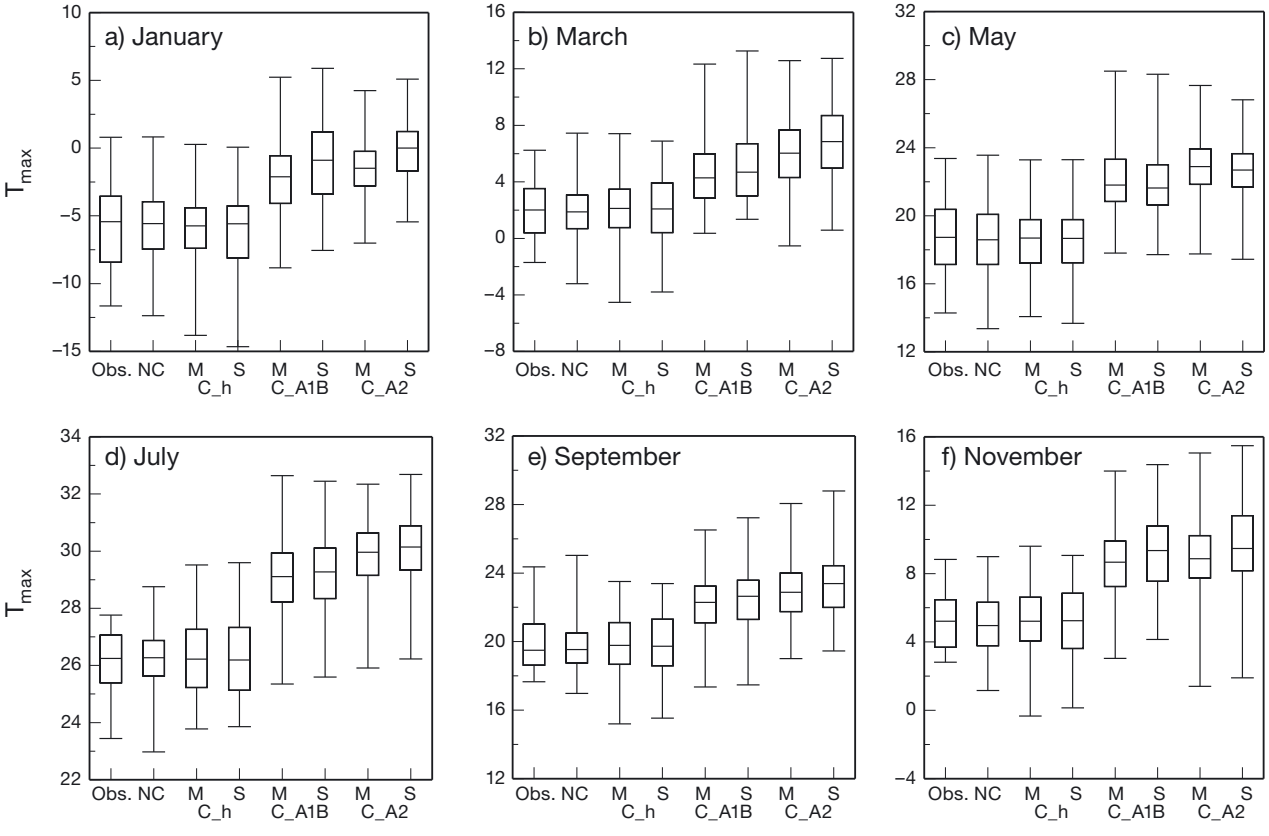

Fig. 7. Monthly mean daily T_{max} of the observations (Obs.) and the NC and C_h, C_A1B, and C_A2 at Site 7 (see Table 2) using the MMSDM with the modified randomization procedure and the SSDM with the previously developed randomization procedure for each month, where 'M' and 'S' represent MMSDM and SSDM, respectively. For brevity, only results for (a) January, (b) March, (c) May, (d) July, (e) September, and (f) November are shown. The results of all SDMs are based on 50 realizations. Box-whisker plots: minimum, lower quartile, median, upper quartile and maximum values. Abbreviations in Table 1

larger than those with the MMSDM. These large increases in monthly mean daily T_{max} are likely an effect of the uncontrolled variances in the deterministic series of the C_A1B(S) and C_A2(S).

Fig. 8 displays the monthly SDs of daily T_{max} of the observations and the NC and C_h, C_A1B, and C_A2 series by the 2 SDMs for each month at Site 7. The NC reproduced the observation variables very well for each month, as well as the C_h(M)s. The differences in the medians of C_A1B(M) and C_h(M) varied from −0.6 to 0.3°C and those between C_A2(M) and C_h(M) varied from −0.7 to 0.4°C. The results of the SSDM showed worse reproduction ability than that of the MMSDM, especially in January, February, March, and November in terms of the median and first and third quartiles. As shown in Fig. 4, the variances of the deterministic series with the CGCM3 historical predictors are larger than those of the observation series, especially in winter, and the variance inflation methodology of the SDSM and ASD could not adjust the deterministic series driven by the CGCM3 historical and future predictors. C_A1B(S) and C_A2(S) produced larger values for the statistic than C_A1B(M) and C_A2(M) in January, February, and November.

Fig. 9 presents the seasonally calculated 90th percentile of daily T_{max} and 10th percentile of daily T_{min} in summer and winter at Site 7. The extreme variables reproduced by the NC showed relatively good performance as for the MMSDM, i.e. C_h(M). The medians are 2.6 to 4.1°C and 3.1 to 5.2°C higher for $T_{max}90$ while 2.0 to 4.7°C and 2.5 to 5.6°C higher for $T_{min}10$ with C_A1B and C_A2, respectively, than those with C_h. The C_h(S) results with the SSDM showed an overestimation (underestimation) of the $T_{max}90$ ($T_{min}10$) in winter. The series projected by the SSDM (C_A1B(S)) and C_A2(S)) yielded a larger increase for the extremes than those by MMSDM (C_A1B(M)) and C_A2(M)) in winter.

Fig. 10 presents the percentages of the hot days in summer (HD90) and cold days in winter (CD10) at Site 7. The extreme variables reproduced by the NC showed relatively good performance as for the MMSDM with CGCM3 predictors, i.e. C_h(M). The

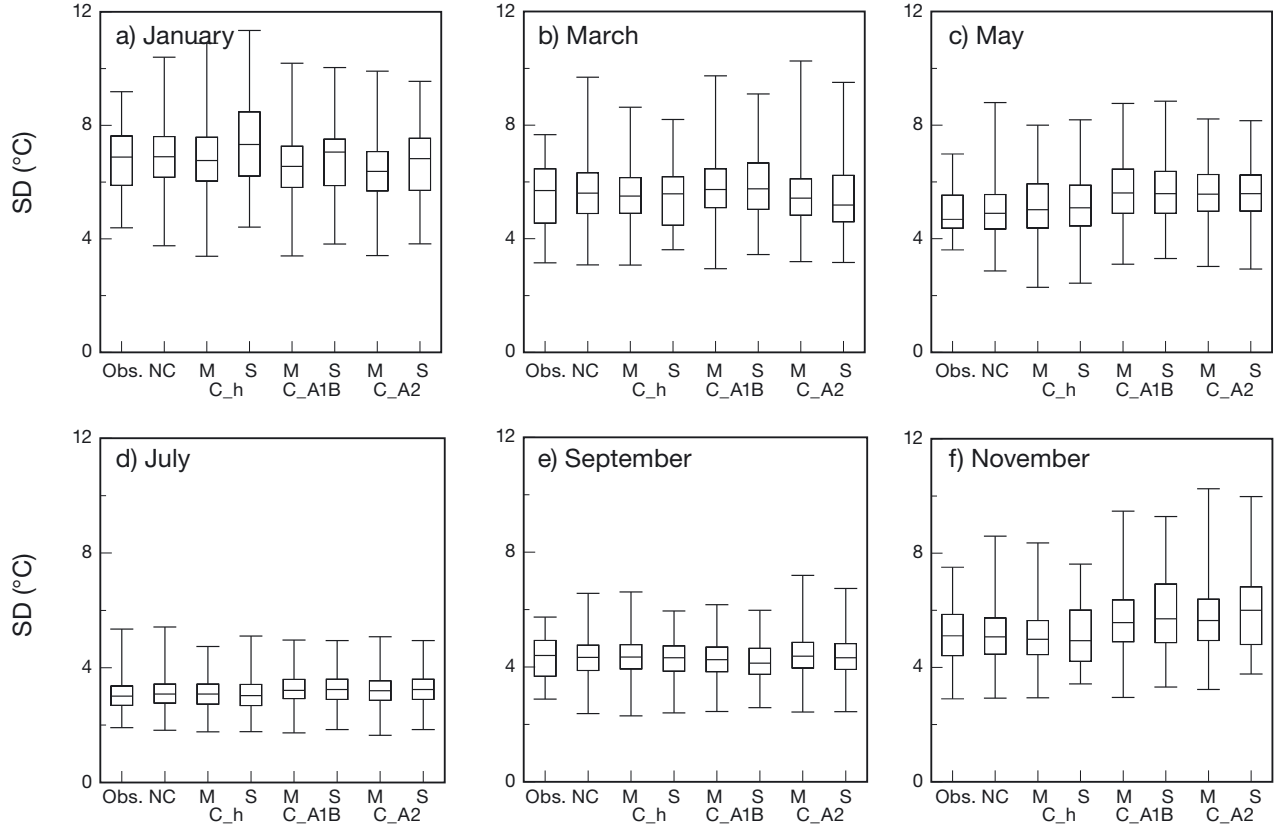

Fig. 8. Monthly SDs of the daily T_{max} of the observation (Obs.) and the NC and C_h, C_A1B, and C_A2 at Site 7 (see Table 2) using the MMSDM with the modified randomization procedure (M) and the SSDM with the previously developed randomization procedure (S) for each month. For brevity, only results for (a) January, (b) March, (c) May, (d) July, (e) September, and (f) November are shown. The results of all SDMs are based on 50 realizations. Abbreviations in Table 1

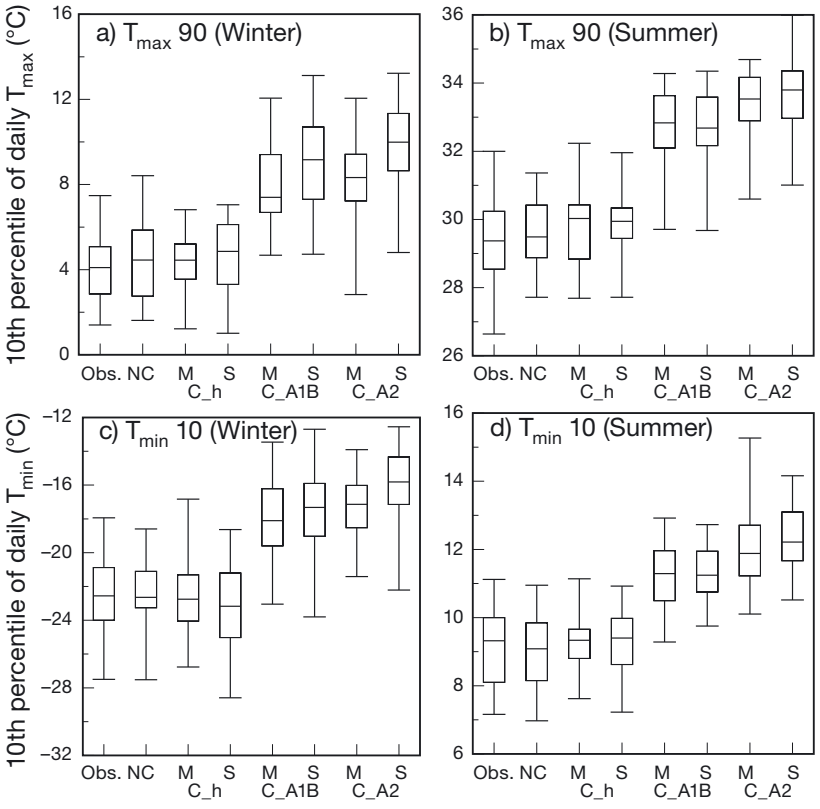

Fig. 9. 90th percentile of daily T_{max} and 10th percentile of daily T_{min} values from the observations (Obs.) and the NC and C_h, C_A1B, and C_A2 at Site 7 (see Table 2) using the MMSDM with the modified randomization procedure (M) and the SSDM with the previously developed randomization procedure (S) in winter and summer. Abbreviations in Table 1

C_h(S) results with the SSDM showed an overestimation of the CD10. The series projected by the SSDM (C_A1B(S)) and C_A2(S)) yielded slightly larger increase for HD90 but larger decreases for CD10 than those by MMSDM (C_A1B(M)) and C_A2(M)). As for the other extremes of temperatures (T_{min}10 and T_{max}90), both SSDM and MMSDM models project a systematic higher increase for the A2 scenario than the A1B one, for both summer and winter seasons.

Fig. 11 presents the differences in the average values of the monthly means of all observation sites between 2 projected series (C_A1B(M)) and C_A2(M)) and the historical series (C_h(M)) that are obtained using the MMSDM with the post-adjustment scheme. In Fig. 11, the projected series of C_A1B yielded monthly means 2.0 to 4.7°C larger than the series downscaled by C_h for T_{max} and T_{min} for each month. The differences are larger in winter than in the other seasons for both T_{max} and T_{min}. In January, February, March, July, and December, the increases of T_{min} are larger than that of T_{max}. As shown also in Fig. 11, the projected series of C_A2 yielded values 2.7 to 5.4°C larger than the series downscaled by C_h for T_{max} and T_{min} for each month. The monthly means of T_{max} and T_{min} with C_A2 are larger than those with C_A1B for all months. This higher warming with the A2 emission scenario (versus the A1B scenario) is compatible with the range of warming suggested by all AOGCMs at the global scale as well as over North America (see IPPC 2007, Christensen et al. 2007). Also, in the study of Gachon & Dibike (2007) using SDSM over northern Canada, the MMSDM is better able to reproduce this higher warming in winter than in the other seasons based on the higher SRES emission scenario after 2050 (see Nakicenovic et al. 2000).

In Fig. 11, T_{max} and T_{min} differences between the averages of the monthly means at the 4 AOGCM grid points (see GP1–GP4 grid points in Fig. 1) in the future (2061–2100) series and the historical (1961–2000) series from the raw CGCM3 outputs with the A2 SRES scenario (CGCM3, A2) are also provided. In most months, the T_{max} and T_{min} series projected by the raw CGCM3 outputs showed larger increases than with the MMSDM with the CGCM3 atmospheric predictors, especially in the winter season (December, January, February, and March). However, these differences between winter and the other seasons projected by the CGCM3 model versus the MMSDM model are larger, as the BAF and DAF values were also more distinctly different from 0 and 1, respectively (see Fig. 4) for these winter months, especially for T_{min}. This means that the corrected predictor biases for these months in the MMSDM model were more prominent than for the other months, inducing higher differences with respect to the raw CGCM3 climate change signals.

Table 4 lists the average values of the temperature indices at the 10 observation sites, where the MMSDM is used for C_h, C_A1B, and C_A2. Here, the differences in the indices between the projected series (C_A1B and C_A2) and historical series (C_h) are also provided. For T_{max}90, NC and C_h reproduced this temperature index quite well, and differences between observation and the 2 downscaled series are <0.5°C. In the future, increases in this index are larger in winter and spring than in summer and

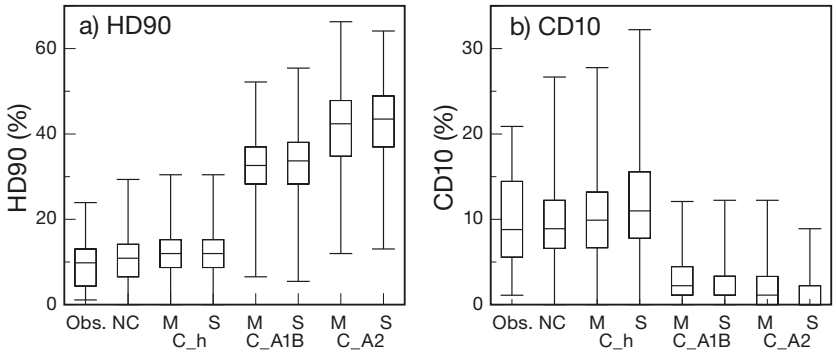

Fig. 10. HD90 and CD10 from the observations (Obs.) and the NC and C_h, C_A1B, and C_A2 at Site 7 (see Table 2) using the MMSDM with the modified randomization procedure (M) and the SSDM with the previously developed randomization procedure (S) for each season. Abbreviations in Table 1

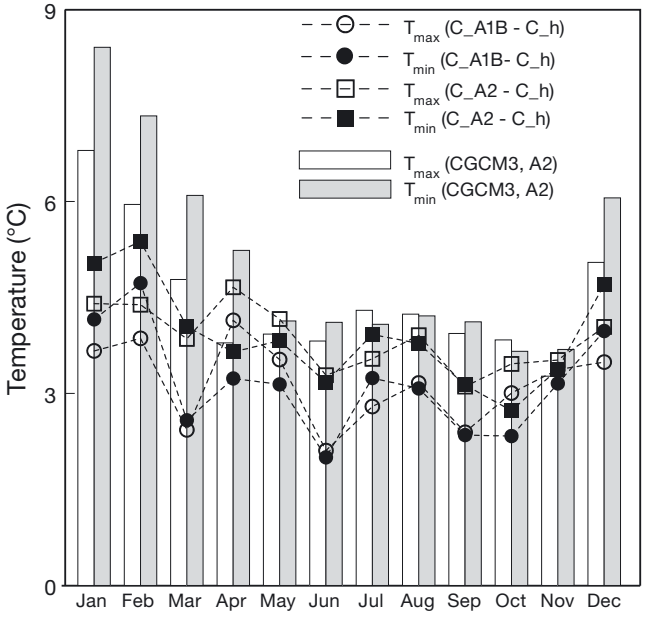

Fig. 11. Daily T_{max} and T_{min} differences between the averages of the monthly means at the 10 observation sites in the projected series (C_A1B and C_A2) and the historical series (C_h) downscaled by the MMSDM. T_{max} and T_{min} differences between the averages of the monthly means at the 4 AOGCM grid points (see GP1–GP4 grid points in Fig. 1) in the future (2061–2100) and the historical (1961 –2000) series from the raw CGCM3 outputs with the A2 SRES scenario (CGCM3, A2) are also provided. Abbreviations in Table 1

autumn, as also noted in the mean daily T_{max} values for both C_AlB and C_A2 (see Fig. 11). For $T_{min}10$, NC and C_h also reproduced this index quite well, and differences between observation and the 2 downscaled series are <0.3°C. C_A1B and C_A2 yielded warming values 2.1 to 4.5°C and 2.7 to 5.8°C larger than C_h, respectively. The $T_{min}10$ of C_A1B and C_A2 showed also the largest increase in winter, and higher than for the $T_{max}90$ for this last season. For the HD90 and CD10, the NC and C_h reproduced these indices reasonably well, and the differences between observation and the 2 downscaled series are <2% (<2 d within a season of 90 d). In the future, under warming climate conditions, C_A1B and C_A2 yielded 19.6 and 28.0% more hot days whereas 6.7 and 7.5% fewer cold days than C_h. For the mean of diurnal temperature range (DTR), NC and C_h also reproduced this index quite well, with differences between observation and the 2 downscaled series <0.3°C. For this index, C_A1B and C_A2 yielded 0.4 and 0.3°C larger values than C_h in spring and autumn, whereas they yielded smaller values than historical runs in winter and summer. As shown in Fig. 11, the weaker increases in T_{min} with C_A1B and C_A2 than those in T_{max} in April, May, June, October, and November, could favor a future increase in DTR in spring and autumn. The NC and C_h reproduced the FSL and GSL quite well, with differences between observations and the 2 downscaled series <2 d for both indices. In the future, C_A1B and C_A2 simulations suggest a decrease in the FSL values by 23 and 28 d, respectively, and an increase in the GSL values by 23 and 27 d, respectively.

4. DISCUSSION

Although regression-based SDMs are developed using empirical relationships between local-scale predictands and large-scale observed data over the historical period, i.e. using reanalysis climate variables (Wilby & Dawson 2004), future downscaled series are developed using atmospheric predictors from an AOGCM. This is realized under the assumption that changes of the large-scale predictors simulated by the considered AOGCM are robust, physically sensible, and are able to capture the main signals of anticipated changes, including multiyear variability of the local-scale predictands (i.e. T_{max} and T_{min} in our case). However, the AOGCM predictors are not free of biases, especially for variables near the surface. In general, AOGCMs are thought to give a more realistic description of the free tropospheric variables and large-scale circulation than of surface parameters (e.g. Murphy 1999, Gachon & Dibike 2007). Stochastic weather generators and weather typing approaches

Table 4. Average values of the temperature indices calculated from the observed series (Obs.), the downscaled series (NC and C_h), and the projected series (C_A1B, and C_A2) at the 10 sites. All differences of C_A1B – C_h and C_A2 – C_h are statistically significant based on a 2-sample *t*-test at a 5% significance level. Abbreviations in Table 1

Index	Season	Obs.	NC	C_h	C_A1B	C_A2	C_A1B – C_h	C_A2 – C_h
T_{max}90 (°C)	Winter	4.05	4.54	4.11	7.72	8.35	3.62	4.25
	Spring	22.03	21.81	21.65	26.17	26.41	4.52	4.76
	Summer	29.38	29.70	29.81	32.54	33.51	2.73	3.71
	Autumn	22.61	22.33	22.54	24.94	25.96	2.39	3.41
T_{min}10 (°C)	Winter	–23.40	–23.13	–23.27	–18.75	–17.49	4.51	5.77
	Spring	–10.62	–10.63	–10.41	–8.18	–6.67	2.23	3.74
	Summer	8.90	8.87	8.99	11.11	11.74	2.12	2.75
	Autumn	–4.71	–4.92	–4.73	–2.29	–2.04	2.44	2.69
HD90 (%)	Summer	9.43	10.65	11.41	31.04	39.45	19.63	28.03
CD10 (%)	Winter	9.70	9.02	9.37	2.69	1.90	–6.68	–7.47
DTR (°C)	Winter	8.84	9.19	9.15	8.63	8.50	–0.52	–0.65
	Spring	10.05	10.20	10.11	10.49	10.50	0.38	0.38
	Summer	10.61	10.67	10.66	10.57	10.61	–0.08	–0.05
	Autumn	8.72	8.83	8.83	9.13	9.12	0.30	0.29
FSL (d)	Annual	155	157	154	131	125	–23	–28
GSL (d)	Annual	204	203	205	228	232	23	27

are not free from biases resulting from low level atmospheric biases, as they generally employ differences (delta) on raw surface temperature and precipitation outputs projected by AOGCMs without any de-biased factors to generate future regional series. These potential biases in low level atmospheric variables (i.e. in our case 1000 and 850 hPa fields used as predictors, see Table 3) should propagate within the downscaling process, justifying the use of a post-adjustment procedure as in the present study. This has the advantage of preventing the propagation of potential misrepresentative atmospheric information in the downscaled climate change values. Therefore, there are seasonal differences in the atmospheric forcing factors and their combined effects on the T_{max} and T_{min} variability across the year. Indeed, as there is some intra-annual variability in the large-scale atmospheric circulation and in the regional forcing factors due for example to surface conditions (i.e. snow cover, frost/thaw conditions of the soil and its influence on the water phase and cycle), different predictors and regression parameters for each month are needed (Jeong et al. 2012c). This implicates a variable post-adjustment procedure developed per month, along with an in-depth analysis of AOGCM outputs at the space and time scales of use during the SDM model development (see the detailed evaluation using the CGCM3 predictors over eastern Canada in Jeong et al. 2012b).

The previously proposed single post-adjustment scheme employed by the SDSM and ASD had difficulty reproducing the observed temperature variance and extreme characteristics, especially in winter. Gachon & Dibike (2007) and Hessami et al. (2008) previously described these systemic differences between observations and downscaled values over various areas of northern and eastern Canada. As also demonstrated by Jeong et al. (2013) and in the present study, the modified post-adjustment scheme was able to improve the simulated variances and extreme characteristics of the predictands with respect to observed values, for all seasons or months. This post-adjustment procedure developed over the current period is assumed to be valid in the future. As suggested in Fig. 11, the effect of these monthly based correction functions on the T_{min}/T_{max} climate change values is in part responsible for higher differences in the local-scale climate change signals between the MMSDM model and the CGCM3 raw outputs during the winter months. During this last season, some distinctive lower warming values are obtained from the MMSDM model, as the BAF and DAF were more noticeably different from 0 and 1 than for the other months (see Fig. 4). These differences could also be in part due to non-stationary biases of the CGCM3 model, and/or misleading in the regional scale predictors or feedbacks simulated by this AOGCM and within the downscaling procedure itself using only coarse-scale atmospheric variables.

In Table 5, we briefly examine the likelihood of our projected temperature regimes with respect to the

range of anticipated warming values from an ensemble of various AOGCMs and 1 RCM simulation over the target area. For the daily T_{max}, our projected warming results are within the range of the mean ensemble AOGCM projections (8 A2 runs obtained over Canada from the CCCSN, www.cccsn.ec.gc.ca) which are around 4.5°C in average in winter (with a range of 1.2 to 6.4°C between models and DJF months), and with a smaller increase in summer of 4°C on average (with a range of 1.8 to 6.3°C between models and JJA months). Indeed for our downscaled values, T_{max} increases by around 4.4°C in winter and by around 3.5°C in summer (see Table 5). This is also compatible with the range of warming projected by a simulation of the Canadian RCM (CRCM4.2.3 driven by the same run of the CGCM3 model as for the MMSDM model) during winter, i.e. around 5°C. However, in summer a higher T_{max} signal of around 5.3°C is suggested from the CRCM (mainly from highest warming appearing during July and August). For the ensemble mean of AOGCMs and for the daily T_{min}, the warming is around 6.4°C in winter (with a range of 2.5 to 10.4°C between models and DJF months), with the smallest increase in summer (3.9°C, with a range of 2.7 to 5.6°C between models and JJA months). In our downscaled values, the winter T_{min} increases more moderately than the mean of AOGCMs by around 5.1°C, but with a compatible warming in summer of around 3.8°C (see Table 5), i.e. with also a compatible higher warming than for the daily T_{max} signal values for both seasons. In such a case, the CRCM simulation suggests a distinctive higher increase of 7.1°C in winter and of 4.7°C in summer. In summary, an overall higher warming is generally obtained in winter, spring, and autumn months than in summer months, and for the T_{min} downscaled values with respect to daily T_{max} ones, as for the majority of AOGCMs. This is in good agreement with the variability experienced over the last few decades in eastern Canada (Zhang et al. 2000), and with a general anticipated warming trend over northern countries such as Canada with a reduction

Table 5. Differences between the averages of monthly means in the future series (2071–2099) and the reference series (from 1971–2000) projected by several AOGCMs, MMSDM, and 1 simulation of the Canadian Regional Climate Model (version 4.2.3 driven by CGCM3, i.e. same CGCM3 run as used for the MMSDM) with the A2 SRES scenarios for the target area. All AOGCM and CRCM data have been provided by the Canadian Climate Change Scenarios Network, a project of Environment Canada (see further information at: www.cccsn.ec.gc.ca). Detailed descriptions of the versions and runs of the AOGCMs can be obtained from the IPCC Data Distribution Centre (www.ipcc-data.org/). T_{max}/T_{max}: daily maximum/minimum temperature. Other abbreviations as in Table 1

	Jan	Feb	Mar	Apr	May	Jun	Jul	Aug	Sep	Oct	Nov	Dec
T_{max} (°C)												
CGCM3T47(Mean)	5.75	4.98	3.85	4.18	4.78	3.92	4.55	4.64	4.22	4.74	4.03	4.20
BCM2.0(Run 1)	4.32	1.22	1.63	1.77	4.55	2.77	3.66	3.55	3.97	3.94	2.42	4.69
CGCM3T63(Run 1)	5.83	6.35	5.16	5.11	5.01	4.87	4.62	5.02	4.12	4.44	4.30	4.49
CSIROMk3.0(Run 1)	5.57	5.63	4.79	2.12	2.18	2.04	1.81	3.57	2.56	3.51	3.54	4.28
CSIROMk3.5(Run 1)	3.57	3.43	3.59	3.89	3.82	3.70	4.65	4.12	4.56	3.29	3.81	3.33
INMCM3.0(Run 1)	3.76	4.73	4.25	3.82	2.23	3.18	4.86	4.72	4.13	4.24	4.09	4.28
MIROC3.2 (Mean)	5.78	5.95	7.65	6.72	5.07	4.65	6.26	5.72	5.68	5.65	5.30	4.73
NCARPCM(Run 1)	4.21	3.37	2.73	1.39	2.61	3.27	2.81	3.21	4.32	3.23	2.35	2.32
Avg. of the AOGCMs	4.85	4.46	4.21	3.62	3.78	3.55	4.15	4.32	4.19	4.13	3.73	4.04
MMSDM	4.63	4.41	3.36	5.01	4.25	3.08	3.44	4.08	3.57	3.77	3.33	4.09
CRCM4.2.3(Run 1)	5.19	5.16	3.78	5.46	4.36	4.65	6.56	7.91	6.70	4.76	3.52	4.63
T_{min} (°C)												
CGCM3T47(Mean)	7.35	6.28	5.27	5.56	5.01	3.85	4.38	4.33	4.43	4.56	4.14	5.39
BCM2.0(Run 1)	6.30	2.52	3.62	1.99	3.78	2.72	3.36	3.49	4.37	3.33	3.37	6.54
CGCM3T63(Run 1)	8.53	8.63	7.91	6.49	5.17	4.55	4.46	4.97	4.03	4.43	4.63	6.35
CSIROMk3.0(Run 1)	10.14	10.39	6.27	1.60	2.30	2.25	2.09	3.60	2.52	3.03	3.62	6.85
CSIROMk3.5(Run 1)	5.68	5.41	3.38	3.35	3.58	3.69	4.94	4.59	4.98	3.53	3.04	4.35
INMCM3.0(Run 1)	5.46	5.72	5.94	6.02	3.33	2.89	4.45	4.99	4.15	4.54	4.59	5.42
MIROC3.2 (Mean)	8.77	8.45	8.27	6.35	4.99	4.43	5.63	5.25	5.13	4.95	4.82	6.21
NCARPCM(Run 1)	5.25	4.64	4.53	1.83	2.99	2.83	2.84	2.81	3.67	3.03	3.39	3.42
Avg. of the AOGCMs	7.18	6.51	5.65	4.15	3.89	3.40	4.02	4.25	4.16	3.92	3.95	5.57
MMSDM	5.23	5.39	3.54	3.85	3.92	3.08	3.82	3.91	3.53	2.99	3.27	4.70
CRCM4.2.3(Run 1)	7.68	6.97	6.04	6.48	4.76	4.15	4.89	5.19	5.05	4.21	4.02	6.75

of the snow cover season and ground frost conditions in the future (see Christensen et al. 2007). More differences in the inter-seasonal changes and in the monthly features of the T_{max} and T_{min} projected values (with the highest monthly mean signal appearing in August for T_{max}) are suggested by the CRCM, but these are not fully compatible with AOGCMs and MMSDM projections.

As noted in various recent studies on the evaluation of climate model biases (Piani et al. 2010, Maraun 2012, Teutschbein & Seibert 2012), if the biases are not stable (i.e. not stationary), the error does not cancel out in the differences between the future and current simulated periods (i.e. delta methods), and the signal should incorporate various parts of the biases. As shown in the recent study by Maraun (2012) using RCM ensemble simulations in Europe, for winter temperatures over high elevation or over snow/sea-ice surface conditions, bias changes in RCMs are mainly caused by a biased forcing sensitivity of surface albedo or surface conditions. This is also true in Canada over snow, sea-ice, and heterogeneous land surface conditions (see the work over northern Canada by Gachon & Dibike 2007) which are not well simulated by AOGCMs or RCMs and where the feedbacks are strong, and not homogeneous and linear with time. For example, a known warm bias is present in the simulated daily T_{max} values in summertime in the CRCM (the version presented in Table 5) over our target region (see Fig. 12 in Eum et al. 2012). This is also the case in the low level air temperature of the CGCM3 in winter/summer months (for example a cold bias of around 3°C is present in these seasons for the simulated daily T_{max} with respect to observed data over the target area; not shown). This inconsistency may pose severe constraints on the usefulness of AOGCM or RCM information (and the derived delta values) used at the local scale, especially in regions characterized by complex physiographic settings or where regional or local forcing play a key role in the temperature regime at the seasonal, monthly, and daily scales (and this varies between T_{min} and T_{max}, such as noted in the variation in the S^{NC} standard deviation of the residuals of the series of predictands in Fig. 3). Hence, there is still a mismatch of scales, especially for meso- and small-scale processes, that are often not captured at the RCM/AOGCM grid cell, and this led to the development of bias correction approaches. However, although bias correction is often mandatory to provide more realistic climate simulations for impact studies, it is also a controversial subject (Ehret et al. 2012, Muerth et al. 2012), despite its advantageous ability to reduce biases in climate model outputs and in their climate change information (see Teutschbein & Seibert 2012). In our case, the usefulness of the correction functions for AOGCM biased predictors in the MMSDM model needs to be tested in further work over conditions differing from those for which it was calibrated, i.e. to deal with changing climate conditions and possible changes in bias relationships. The MMSDM methodology suggested here is relatively more robust and provides more plausible signals than the use of the CGCM3 raw outputs at the local scale. However, this downscaling model may be conservative with regards to stationarity in the correction functions applied for the CGCM3 predictor values. Hence, more work is needed to analyze the performance of the suggested correction functions for its more general use with simulations under changed conditions.

5. CONCLUSIONS

This study developed a new randomization procedure with a modified post-adjustment scheme for the multivariate multi-site statistical downscaling model (MMSDM) to overcome the systematic error originating from differences between the NC and AOGCM historical predictors and their use in the downscaling of daily surface predictands (i.e. T_{max} and T_{min}) at multiple observation sites. The modified post-adjustment scheme employs a DAF to preserve the proportion of variances in deterministic components driven by large-scale AOGCM predictors and that of random noise in the downscaled scenarios. Therefore, the new randomization procedure can control the systematic errors in the series predicted by the AOGCM historical predictors, and also prevent the propagation of errors into the future predictand values.

The series downscaled by the MMSDM with the CGCM3 historical predictors reproduced the estimated correlation coefficients among the observed cross-site and at-site T_{max} and T_{min} almost exactly. The result implies that the MMSDM model reproduces quite well the covariance structure of the observations. For all observation sites, the series downscaled by the MMSDM and both NC predictors and CGCM3 historical predictors reproduced the basic statistics (monthly means and standard deviations) and extreme indices of the observed daily T_{max} and T_{min} series. Furthermore, the series projected by the MMSDM with the CGCM3 A1B and A2 predictors are able to capture the systematically higher climate warming (both mean and extreme seasonal regimes) corresponding to the A2 than the A1B emis-

sion scenario in all seasons and runs, and for all stations analyzed.

On average at the 10 observation sites, the monthly means of daily T_{max} and daily T_{min} increased by 2.0 to 4.7°C in the CGCM3 A1B future scenarios, whereas they increased by 2.7 to 5.4°C in the A2 future scenarios. The projected daily temperature series showed a greater increase in winter than in the other seasons, and in T_{min} than in T_{max}. The 90th percentile of T_{max} and the 10th percentile of T_{min} showed higher increases in spring and in winter than in the other seasons in the future. The mean diurnal temperature ranges (DTRs) of the future C_A1B and C_A2 series showed small increases only in spring and autumn. Consequently, future C_A1B and C_A2 projected increases of hot extreme days in summer but decreases of cold extreme days in winter. The projected future C_A1B and C_A2 series yielded FSL values 23 and 28 d shorter, respectively, than the historical series, whereas they yielded GSL values 23 and 27 d longer.

This study provides an assessment of the effects of climate changes on mean and extreme temperatures over the Montréal area based only on the A1B and A2 atmospheric scenarios from the CGCM3 model. In future work, the MMSDM will be applied to other atmospheric predictors simulated using different emission scenarios and different AOGCMs. Although perturbed ensemble scenarios based on the randomization process of the MMSDM were provided, the limited ensemble describes only the unexplained uncertainty by the linear transfer function of the MMSDM under the CGCM3 future predictors. Therefore, a multi-model ensemble approach would be necessary to quantify other sources of uncertainty (e.g. uncertainties arising from future emission scenarios, internal climate variability, or modeling errors in the AOGCMs) in the climate change information developed over the study area. The MMSDM approach could be applied to simultaneous downscaling of daily temperature and precipitation series on multiple observation sites for a local region where the 2 climate variables have significant temporal and spatial correlations. Therefore, as suggested in the recent work of Teutschbein & Seibert (2012), to test the MMSDM model's ability to perform under shifting conditions, we could evaluate in further works the effect on the downscaled variables when the model is then calibrated over the period with one condition and validated on the period with the other conditions (e.g. a warm versus a cold or a wet versus a dry period). This could further infer the robustness in the post-adjustment procedure of the AOGCM predictors within the MMSDM model.

Acknowledgements. We acknowledge the financial support provided by the Natural Sciences and Engineering Research Council (NSERC) of Canada. We also thank the Data Access Integration (DAI, see http://loki.qc.ec.gc.ca/DAI/) Team for providing the predictor data and technical support. The DAI data download gateway is made possible through collaboration among the Global Environmental and Climate Change Centre (GEC3), the Adaptation and Impacts Research Division (AIRD) of Environment Canada, and the Drought Research Initiative (DRI). We also acknowledge the Canadian Climate Change Scenarios Network (CCCSN) project of Environment Canada, which supports climate change impact and adaptation research in Canada and other partner countries through the provision of AOGCM scenarios, RCM scenarios, and downscaling tools. The CRCM time series data were generated and supplied by the Ouranos Climate Simulations Team.

LITERATURE CITED

Bell JL, Sloan LC, Snyder MA (2004) Regional changes in extreme climatic events: a future climatic scenario. J Clim 17:81–87

Burton A, Kilsby CG, Fowler HJ, Cowpertwait PSP, O'Conell PE (2008) Rainsim: a spatial-temporal stochastic rainfall modeling system. Environ Model Softw 23:1356–1369

Cannon AJ, Whitfield PH (2002) Downscaling recent streamflow conditions in British Columbia, Canada using ensemble neural network models. J Hydrol (Amst) 259: 136–151

Christensen JH, Hewitson B, Busuioc A, Chen A and others (2007) Regional Climate Projections. In: Solomon S, Qin D, Manning M, Chen Z and others (eds) Climate change 2007: the physical science basis. Contribution of Working Group I to the Fourth Assessment Report of the Intergovernmental Panel on Climate Change. Cambridge University Press, Cambridge

Cubasch U, Meehl GA, Boer GJ, Stouffer RJ and others (2001) Projections of future climate change. In: Houghton JT, Ding Y, Griggs DJ, Noguer M and others (eds) Climate change 2001: the scientific basis. Contribution of Working Group I to the Third Assessment Report of the Intergovernmental Panel on Climate Change. Cambridge University Press, Cambridge

Easterling DR (1999) Development of regional climate scenarios using a downscaling approach. Clim Change 41: 615–634

Ehret U, Zehe E, Wulfmeyer V, Warrach-Sagi K, Liebert J (2012) HESS Opinions 'Should we apply bias correction to global and regional climate model data?' Hydrol Earth Syst Sci 16:3391–3404

Eum HI, Gachon P, Laprise R, Ouarda TBMJ (2012) Evaluation of regional climate model simulations versus gridded observed and regional reanalysis products using a combined weighting scheme. Clim Dyn 38:1433–1457

Flato GM, Boer GJ (2001) Warming asymmetry in climate change simulations. Geophys Res Lett 28:195–198

Fowler HJ, Kilsby CG, O'Connel PE, Burton A (2005) A weather-type conditioned multi-site stochastic rainfall model for the generation of scenarios of climatic variability and change. J Hydrol (Amst) 308:50–66

Gachon P, Dibike YB (2007) Temperature change signals in northern Canada: convergence of statistical downscaling results using two driving GCMs. Int J Climatol 27: 1623–1641

Giorgi F, Hewitson B, Christensen J, Hulme M and others

(2001) Regional climate information — evaluation and projections. In: Houghton JT, Ding Y, Griggs DJ, Noguer M and others (eds) Climate change 2001: the scientific basis. Contribution of Working Group I to the Third Assessment Report of the Intergovernmental Panel on Climate Change. Cambridge University Press, Cambridge

Hessami M, Gachon P, Ouarda TBMJ, St-Hilaire A (2008) Automated regression-based statistical downscaling tool. Environ Model Softw 23:813–834

Huziy O, Sushama L, Khaliq MN, Laprise R, Lehner B, Roy R (2013) Analysis of streamflow characteristics over Northeastern Canada in a changing climate. Clim Dyn 40: 1879–1901

IPCC (2007) Climate change 2007: the physical science basis. Summary for policy makers. Contribution of Working Group I to the Fourth Assessment Report of the Intergovernmental Panel on Climate Change. Solomon S, Qin D, Manning M, Chen Z and others (eds) Cambridge University Press, Cambridge

IPCC (2012) Managing the risks of extreme events and disasters to advance climate change adaptation. A Special Report of Working Groups I and II of the Intergovernmental Panel on Climate Change. Field CB, Barros V, Stocker TF, Qin D and others (eds). Cambridge University Press, Cambridge

Jeong DI, Daigle A, St-Hilaire A (2012a) Development of a stochastic water temperature model and projection of future water temperature and extreme events in the Ouelle River basin in Quebec, Canada. River Res Appl doi:10.1002/rra.2574

Jeong DI, St-Hilaire A, Ouarda TBMJ, Gachon P (2012b) CGCM3 predictors used for daily temperature and precipitation downscaling in southern Québec, Canada. Theor Appl Climatol 107:389–406

Jeong DI, St-Hilaire A, Ouarda TBMJ, Gachon P (2012c) A multivariate multi-site statistical downscaling model for daily maximum and minimum temperatures. Clim Res 54:129–148

Jeong DI, St-Hilaire A, Ouarda TBMJ, Gachon P (2012d) Multisite statistical downscaling model for daily precipitation combined by multivariate multiple linear regression and stochastic weather generator. Clim Change 114: 567–591

Jeong DI, St-Hilaire A, Ouarda TBMJ, Gachon P (2013) Projection of future daily precipitation series and extreme events by using a multi-site statistical downscaling model over Montréal, Québec, Canada. Hydrol Res 44:147–168

Kalnay E, Kanamitsu M, Kistler R, Collins W and others (1996) The NCEP/NCAR 40-year reanalysis project. Bull Am Meteorol Soc 77:437–471

Katz RW, Brown BG (1992) Extreme events in a changing climate: variability is more important than averages. Clim Change 21:289–302

Khalili M, Nguyen VVT, Gachon P (2013) A statistical approach to multi-site multivariate downscaling of daily extreme temperature series. Int J Climatol 33:15–32

Kilsby CG, Jones PD, Burton A, Ford AC and others (2007) A daily weather generator for use in climate change studies. Environ Model Softw 22:1705–1719

Kistler R, Kalnay E, Collins W, Saha S and others (2001) The NCEP/NCAR 50-Year Reanalysis. Bull Am Meteorol Soc 82:247–267

Lobell DB, Bonfils C, Duffy PB (2007) Climate change uncertainty for daily minimum and maximum temperatures: a model inter-comparison. Geophys Res Lett 34:L05715 doi:10.1029/2006GL028726

Maraun D (2012) Nonstationarities of regional climate model biases in European seasonal mean temperature and precipitation sums. Geophys Res Lett 39: L06706, doi:10.1029/2012GL051210

Meehl GA, Zwiers F, Evans J, Knutson T, Mearns L, Whetton P (2000) Trends in extreme weather and climate events: issues related to modeling extremes in projections of future climate change. Bull Am Meteorol Soc 81: 427–436

Meehl GA, Stocker TF, Collins WD, Friedlingstein P and others (2007) Global climate projections. In: Solomon S, Qin D, Manning M, Chen Z and others (eds) Climate change 2007: the physical science basis. Contribution of Working Group I to the Fourth Assessment Report of the Intergovernmental Panel on Climate Change. Cambridge University Press, Cambridge

Mehrotra R, Sharma A (2007) Preserving low-frequency variability in generated daily rainfall sequences. J Hydrol (Amst) 345:102–120

Muerth MJ, Gauvin St-Denis B, Ricard S, Velazquez JA and others (2012) On the need for bias correction in regional climate scenarios to assess climate change impacts on river runoff. Hydrol Earth Syst Sci Discuss 9:10205–10243

Murphy J (1999) An evaluation of statistical and dynamical techniques for downscaling local climate. J Clim 12: 2256–2284

Nakicenovic N, Alcamo J, Davis G, de Vries B and others (2000) IPCC Special Report on Emissions Scenarios. Cambridge University Press, Cambridge

Piani C, Haerter JO, Coppola E (2010) Statistical bias correction for daily precipitation in regional climate models over Europe. Theor Appl Climatol 99:187–192

Roy P, Gachon P, Laprise R (2012) Assessment of summer extremes and climate variability over the north-east of North America as simulated by the Canadian Regional Climate Model. Int J Climatol 32:1615–1627

Schoof JT, Pryor SC, Robeson SM (2007) Downscaling daily maximum and minimum temperatures in the Midwestern USA: a hybrid empirical approach. Int J Climatol 27: 439–454

Tebaldi C, Hayhoe K, Arblater JM, Meehl GA (2006) Going to the extremes: an intercomparison of model-simulated historical and future changes in extreme events. Clim Change 79:185–211

Tett SFB, Johns TC, Mitchell JFB (1997) Global and regional variability in a coupled AOGCM. Clim Dyn 13:303–323

Teutschbein C, Seibert J (2012) Is bias correction of Regional Climate Model (RCM) simulations possible for non-stationary conditions? Hydrol Earth Syst Sci Discuss 9: 12765–12795

Vescovi L, Rebetez M, Rong F (2005) Assessing public health risk due to extremely high temperature events: climate and social parameters. Clim Res 30:71–78

von Storch H (1999) On the use of 'inflation' in statistical down scaling. J Clim 12:3505–3506

Walther GR, Post E, Convey P, Menzel A and others (2002) Ecological responses to recent climate change. Nature 416:389–395

Wilby RL, Dawson CW (2004) Using SDSM Version 3.1 — a decision support tool for the assessment of regional climate change impacts. User manual. Available at http://unfccc.int/resource/cd_roms/na1/v_and_a/Resoursce_materials/Climate/SDSM/SDSM.Manual.pdf

Zhang X, Vincent LA, Hogg WD, Niitsoo A (2000) Temperature and precipitation trends in Canada during the 20th century. Atmos-Ocean 38:395–429

Editorial responsibility: Balaji Rajagopalan, Boulder, Colorado, USA

Submitted: September 26, 2012; Accepted: February 21, 2013
Proofs received from author(s): May 11, 2013